Field measurements of snowpack response to explosive loading

Stephan Simioni [a,*], Rolf Sidler [b], Jürg Dual [c], Jürg Schweizer [a]

[a] WSL Institute for Snow and Avalanche Research SLF, Davos, Switzerland
[b] Simon Fraser University, Burnaby, Canada
[c] Institute of Mechanical Systems, ETH Zürich, Switzerland

A B S T R A C T

Avalanche control by explosives is among the key temporary preventive measures. Hitherto, little is known about wave propagation in a snowpack caused by an explosion. During the winter 2013–2014 we performed field experiments on a flat study site. We triggered slurry explosive charges at different heights above the snow surface. At three different distances from the point of explosion we measured surface air pressure and accelerations of the snowpack at various depths. Cameras were placed in the snow pits for recording weak layer failure and crack propagation. We report empirical relations for the decay of near-surface air pressure, accelerations, displacement velocities and displacement with distance from the explosion and depth within the snowpack. Waves within the snowpack arrived earlier at the sensors than the corresponding air pressure waves at the microphones. Air pressure decayed stronger than accelerations within the snowpack. Weak layer failure mainly happened in the top part of the snowpack. We observed two types of weak layer failure, one caused by the direct impact of the air pressure wave close to the point of observation, the other by failure induced by the air pressure wave closer to the point of explosion and subsequent crack propagation. Our measurements increase the understanding of acoustic wave propagation in snow and can be used for comparison with numerical simulations.

© 2015 The Authors. Published by Elsevier B.V. This is an open access article under the CC BY-NC-ND license (http://creativecommons.org/licenses/by-nc-nd/4.0/).

1. Introduction

Avalanche control by explosives has become a key temporary preventive measure in avalanche mitigation. To protect ski runs, power lines and occasionally exposed parts of settlements, avalanches are triggered artificially – often using explosives – during or shortly after storms (McClung and Schaerer, 2006).

The explosion causes a shock wave that propagates radially outward from the point of the explosion in the air as well as in the snow. With increasing distance from the point of explosion, it eventually behaves like an elastic wave for which the propagation speed is independent of the pressure amplitude (Mellor, 1973). The actual process leading from an explosion to an avalanche is not well understood (Frigo et al., 2012). The induced waves propagating in the snowpack lead to a temporary increase of strain. If the strength of a weak layer within the snowpack is locally exceeded, failure can occur and subsequent crack propagation may lead to the release of a slab avalanche.

Whereas avalanche control is successfully applied in practice — mainly based on extensive experience, few studies, experimental or theoretical, exist that investigated the effect of avalanche control by explosions on a snowpack, and in particular the complex behavior of snow under high dynamic loading. Comparison among the various sets of data

is difficult due to different objectives, varying measurement techniques and snow conditions (Sommerfeld, 1982).

The most extensive study on the effect of explosions affecting the snow cover was performed by Gubler (1977). His experiments included varying explosives, detonation heights and snowpack conditions and the resulting findings are still considered state-of-the-art in avalanche control. One of the most relevant results of Gubler (1977), also stated by Mellor (1973), was the observation that charges triggered above the snowpack are most effective in triggering avalanches.

Johnson et al. (1994) conducted experiments with sheet explosives on the snow surface to mimic plane-wave propagation and measure shock wave attenuation with buried stress gauges and found very high attenuation with distance from the explosion. Ueland (1993) showed that shock waves attenuate faster in isothermal snow whereas there is less attenuation in dry snow (Gubler, 1977).

Experiments with a gas gun revealed that snow compaction due to the explosion depends on initial snow density and that significant strain hardening occurs once a critical density is reached (Johnson et al., 1993). Johnson et al. (1993) and Johnson et al. (1994) focused on the effects at short distances from the blast. Frigo et al. (2012) also focused on short distances and in particular investigated the influence of different explosives and their placement on crater formation. They derived empirical laws for crater depth and diameter. Binger et al. (2006) assessed snowpack compression dependency on detonator orientation. They reported increased layer compression with the blasting cap oriented down.

---

* Corresponding author. Tel.: +41 81 417 0354; fax: +41 81 417 0110.
E-mail address: simioni@slf.ch (S. Simioni).

More recently, Bones et al. (2012) performed tests on dry hard and soft snow slab layers applying the measurement techniques introduced by Tichota et al. (2010) and measured air pressure above the snow surface and accelerations within the snowpack at distances ranging from 3 to 7 m from the point of explosion. They found increasing accelerations in the snowpack with increasing elevation of the explosive charge above the snow surface confirming the findings by Gubler (1977) and Johnson et al. (1994). Bones et al. (2012) showed that attenuation rates of the peak accelerations in the snowpack were largely independent of the distance from the charge. Tichota et al. (2010) concluded that a buried charge does not have a widespread effect beyond the crater in moist snow conditions and mentioned the complex non-linear snow response. Wooldridge et al. (2012) conducted compression tests before and after explosions close to the point of explosion and found that compression test scores decreased. Frigo et al. (2010) performed experiments on a flat field including georadar, seismic and vibration measurements to derive snowpack characteristics, mechanical properties of the snowpack and record wave propagation.

In practice, the key question is to know how far from the point of explosion the snowpack has been sufficiently loaded so that the slope can be considered safe. Gubler (1993) proposed to define the effective range of an avalanche control method to be the radial distance from the point of detonation where the stress at the depth of the weak layer is larger or equal to the load of a skier. Mellor (1973) suggested the stress to be larger than 3.5 kPa, whereas Gubler (1976) considered a value larger than 1 kPa as sufficient to initiate weak layer failure, and eventually release an avalanche. Obviously, the minimal load required to release an avalanche by dynamic explosive loading will depend on the properties of the slab and the weak layer, and a fixed stress value might not fully reproduce the complexity of the problem.

The effect of ground motion induced by an explosive on or above the snowpack on avalanche release has not been investigated in depth. Ground motion might become relevant for avalanche triggering at large distances from an explosion due to the lower attenuation in soil compared to snow. However, amplitudes may not be sufficient at large distances to cause weak layer failure (Ueland, 1993). Based on field experiments, Surinach et al. (2011) concluded that the vibrations of a commonly used gas exploder through the foundation are not sufficient to trigger avalanches beyond the effective range of the system. Chernouss et al. (2006) also investigated the effect of ground motion on avalanche release but due to explosions in an open-pit mine.

Several studies investigated the attenuation of blast noise propagation over snow and bare soil (Albert and Hole, 2001; Albert et al., 2008, 2013). They found that a snowpack significantly increases attenuation of acoustic waves above ground. Johnson et al. (1993) showed the influence of a snow cover on blast noise propagation from C4 charges using microphones at distances ranging from 100 m to 1500 m.

Few studies have tried to model the effect of an explosion on the snowpack. Johnson (1982) used a porous model for wave propagation in snow solving Biot's equations considering the two dilatational waves and the shear wave in snow which are propagating through the ice skeleton and the pore space and which are attenuated differently. Johnson (1990) estimated shock wave attenuation in snow with a momentum model used for porous media. Miller et al. (2011) recently proposed a model for shock wave propagation in and above a snowpack caused by explosions. They showed how stress concentrations around a weak layer develop and compared model results of air pressure to data from an open air blast. Cardu et al. (2008) developed a coupled stress and energy criterion for the artificial release of slab avalanches.

Comprehensive field measurements covering a large range of distances from the point of explosion and measuring the snowpack's response at different distances simultaneously with modern measuring techniques have not been performed so far. Weak layer failure detection in avalanche control experiments was not feasible so far and hence measurements of how weak layers fail caused by an explosion are lacking.

We developed the experimental setup based on the findings by Bones et al. (2012) and Tichota et al. (2010) to measure the influence of an explosion on a seasonal snowpack. During the winter 2013–2014 we performed a series of detailed measurements with commonly employed avalanche control explosives used in Switzerland. Our goal was to measure acoustic wave propagation in the snowpack and to record air pressure and acceleration as a function of charge elevation, charge size, receiver location and snowpack conditions while measuring simultaneously at different distances from the point of explosion. Our results should contribute to an improved understanding of the complex wave propagation principles in a snowpack and serve as a base for modeling. Furthermore, we aimed at introducing a method to detect weak layer failure during avalanche control experiments using explosives.

2. Methods

2.1. Study site

A military firing range in the Swiss Alps directly north of the alpine divide was chosen as study site. The site is characterized by a plane level field with a total area of about 55,000 m^2 at an elevation of 1680 m a.s.l. Roads directly besides the site allow for good accessibility. A flat level study site was chosen to ensure good reproducibility of the experiments; it allows to compare different methods under comparable conditions and to perform safe and precise measurements at the intended location. Flat study sites have already been previously used (e.g., Binger et al., 2006; Bones et al., 2012; Frigo et al., 2010).

2.2. Meteorological conditions during winter 2013–2014

During the winter 2013–2014, snow depth was well above average as recorded at 10 km distance from the study site at the observer station of Splügen (1457 m a.s.l.). The maximum snow depth at Splügen was 144 cm, whereas we recorded a snow depth of up to 187 cm at the study site during the test days directly at the location of the experiments. The relatively thick snowpack did not include any persistent weak layers during the entire winter and can be classified as generally stable (Schweizer and Wiesinger, 2001). The relatively smooth topography was leveled out by snowfall and snow drift. Snow depth varied slightly, but the snowpack layering was spatially rather uniform.

2.3. Experimental data winter 2013–2014

We performed 37 experiments on eight test days with dry (6 days) and wet (2 days) snowpack conditions. For each experiment, we measured air pressure near the snow surface at three different horizontal distances from the point of explosion and snowpack acceleration at approximately the same horizontal distances and three depths within the snowpack (Fig. 1). We recorded high speed videos in each snow pit to perform particle tracking (see below) in order to assess weak layer failure. Coordinates of pit locations were measured by differential GPS at the position of the microphone. Positions of the acceleration sensors were measured relative to the position of the microphone.

2.4. Air pressure measurement

Microphones, as employed by Bones et al. (2012) and Tichota et al. (2010), with an upper pressure limit of 34.5 kPa and manufactured by Larcor were used to measure near-surface air pressure resulting from the explosion at different distances from the point of explosion above the snow surface. For all tests and all pits, air pressure was measured 5 to 10 cm above the snow surface. On one test day, two measurement setups were used in one pit to measure air pressure in addition at 0.96 m above the snow surface.
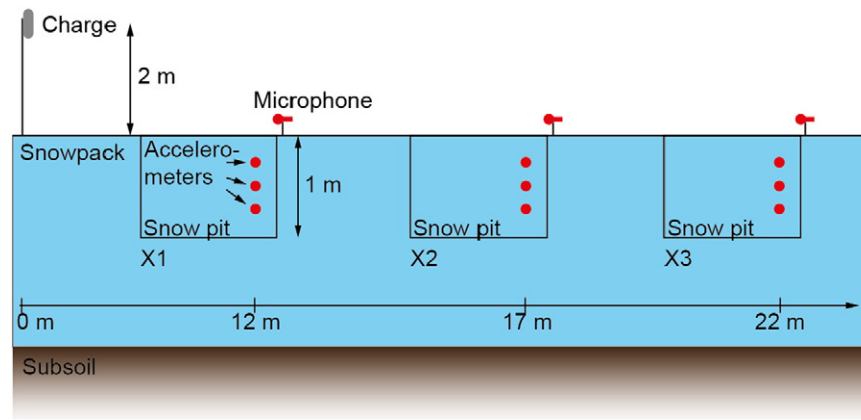
Fig. 1. Longitudinal section of an exemplary measuring layout indicating snow pits X1 to X3 with increasing distance from the point of explosion, charge location, microphones and accelerometers at different distances from the point of explosion and depths within the snowpack. As an example, the charge was elevated at 2 m, the horizontal location of the charge is 0 m, and the snow pits X1 to X3 were located at 12, 17 and 22 m horizontal distance from the point of explosion, respectively. Snow pit depth was usually about 1 m.

Propagation speeds of the air pressure wave were calculated from the air pressure arrival times at the different microphones.

2.5. Acceleration measurement

Two-directional accelerometers (Analog Devices ADXL203, AD22293, AD22037, and ADXL001) were used to measure accelerations within the snowpack (Table 1). All sensors except the ADXL 001 are dual-axis sensors. Two ADXL001 single axis sensors were mounted perpendicularly on a board to be able to measure strong accelerations in two directions. The accelerometers were sealed in foam cylinders in a similar way as described in Gubler (1976); the foam consisted of a two-component mixture with a density corresponding to an average snow density of 200 kg m^{-3} (Fig. 2). We installed the accelerometers within cut-out cavities in the snowpack (Fig. 3) that were slightly smaller in radius at the tip than the sensor to ensure good coupling to the snowpack. A guiding rod was used to place and align the sensor within the cavity. After the measurement the sensors were recovered with a cord fixed to the sensor (Gubler, 1976). Three accelerometers were installed in each snow pit at depths ranging from 0.13 to 0.22 m for the uppermost sensor, 0.43 to 0.53 m for the middle sensor and 0.78 to 0.93 m for the lowest sensor with the exception of one test day when all sensors were buried about 0.35 m deeper than the values given above. Accelerations were measured in radial (horizontal) and vertical directions.

2.6. Recording weak layer failure

Particle tracking has previously been used to record snowpack deformation during snow instability tests (e.g., van Herwijnen et al., 2010). Commodity compact cameras manufactured by GoPro were installed in each snow pit on tripods and recorded the pit wall at 240 frames per second with a resolution of 848 × 480 pixels during the explosion. The specific camera model was chosen due to its low cost, acceptable frame rate and resolution. Markers were installed at the pit walls for particle tracking. The single video stills allowed weak layer failure due to movement of the snowpack to be identified visually. Failure depth within the snowpack can be determined when distances between markers measured at the pit wall change. The time of the explosion was recorded by LED lights flashing at the time of triggering the data acquisition and the explosion.

2.7. Data acquisition

In each snow pit a box containing the data acquisition device and wireless transmission equipment was installed. Data were acquired with several National Instruments cDAQ-9184 (AD converter) recording devices as previously used by Bones et al. (2012) installed in each snow pit. NI 9215 modules were employed to record the signals simultaneously, whereas NI 9402 modules were used for triggering the data acquisition.

Data were recorded at a sampling frequency of 20 kHz and were wirelessly transmitted to a central field computer for data storage. The wireless equipment allowed for efficient installation of the instrumentation and reduced the wired connections to a single data acquisition trigger cable between the snow pits.

2.8. Snowpack characterization

A complete snow profile (Fierz et al., 2009) including layer characteristics and density was recorded on each of the test days in one of the measurement pits. In addition, snow density was measured in each of the three snow pits using a capacity probe (Denoth, 1994). Manual density was also recorded layer by layer if possible. Measurements were taken at intervals of 5 cm or 10 cm starting from close to the snow surface down to the bottom of the pit (approximately 1 m for all experiments) or the bottom of the snowpack. The depth of the pit was chosen with respect to the fact that repeated artificial triggering rarely

Table 1
Accelerometer specifications (www.analog.com).

	ADXL203	AD22293	AD22037	ADXL001-70
Range (g)	+/−1.7	+/−6	+/−18	+/−70
Sensitivity (mV/g)	1000	312	100	24
Resonant frequency (Hz)	5500	5500	5500	>20,000

Fig. 2. Acceleration sensor sealed in foam cylinder (length: 20 cm, diameter: 6 cm).
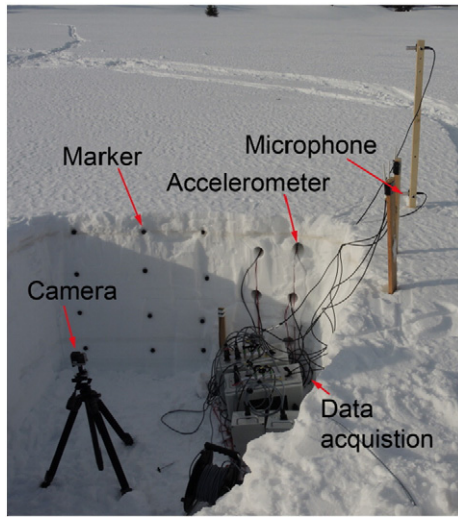
Fig. 3. Measuring equipment in a snow pit. Markers and camera are used for particle tracking velocimetry and failure identification. The three (in this example six) accelerometers are installed within the snowpack in the cavities of the pit wall. The charge is triggered left of the picture and air pressure waves hence propagated through the air from left to right.

leads to large slab thickness and that slab thicknesses involved in skier-triggered avalanches hardly exceed 1 m (van Herwijnen and Jamieson, 2007).

2.9. Explosives and triggering

Slurry explosive charges were used for this study (Table 2). Charge sizes employed in manual avalanche control in Switzerland are in the range of 1.5 to 3.5 kg. Charge sizes installed in fixed avalanche control installations in Europe mainly range between 4.25 and 5 kg.

For the experiments, the explosives were triggered electrically using a blasting machine. The electrical current to ignite the charge was also used to trigger the data acquisition system and to define the time of the detonation.

2.10. Wave arrival time

The arrival time of the wave with the strongest amplitude recorded with the accelerometers and the microphones was determined using an STA/LTA (short time average/long time average) algorithm, where short and long time averages of the signals are compared and a certain threshold is implemented which defines the start (Withers et al., 1998); in addition, the arrival time was checked visually and corrected if required.

3. Results

3.1. Snowpack

The thick snowpack during winter 2013–2014 was relatively warm with snow temperatures in the range of -2 to -1 °C on the days with a dry snowpack. The snowpack was isothermal during the last two test days. Stability tests on the flat study site (Schweizer and Jamieson, 2010) indicated good snowpack stability. A summary of

Table 2
Explosive characteristics.

Explosive name	Alpinit
Explosive type	Slurry
Explosive density (kg m^{-3})	1200
Explosive heat (kJ kg^{-1})	5610
Detonation speed (m s^{-1})	4900

snowpack characteristics is shown in Table 3. Little variation in density was observed between the three density profiles on each test day. Hence the snowpack was considered spatially uniform.

3.2. Air pressure

A typical measurement of near-surface air pressure for three different distances from the point of explosion is shown in Fig. 4. A sharp increase in pressure is followed by a strong decrease and a negative pressure pulse. Finally, a strongly damped oscillation can be observed. Distortion can be seen in the shape of the air pressure wave. Higher frequencies are attenuated more strongly with increasing distance from the point of explosion (Fig. 4). The maximum air pressures of all experiments from winter 2013–2014 are shown in Fig. 5. To compare experiments with different charge sizes, distances were scaled. As we always used the same type of explosives, this was done by scaling the distance x by the cube root of the charge mass m (kg) (Bones et al., 2012; Cooper, 1996):

$$x' = x \, m^{-1/3}. \tag{1}$$

When the air pressure is plotted in a double-logarithmic plot against the scaled distances from the point of explosion, the measurements gather along a straight line suggesting a power law relation (Bones et al., 2012). We therefore fitted a power law to each experiment for the maximum positive p_{max} and negative air pressure p_{min}

$$p = a \, x'^{-b} \tag{2}$$

where x' is the distance from the point of explosion, scaled by the explosive mass (m kg$^{-1/3}$), a and b are parameters. The maximum air pressure decayed with $x'^{-1.1}$ to $x'^{-2.1}$ with a mean exponent b of 1.66 (Fig. 5).

For the first pit, charge elevation was considered in the calculation of the air pressure propagation speed. Propagation speeds reached 547 m s^{-1} for the microphone locations closest to the point of explosion down to 332 m s^{-1} for the largest distances (Table 4).

3.3. Acceleration, displacement velocity and displacement

Vertical accelerations decreased strongly with depth in the snowpack and horizontal distance from the point of explosion (Fig. 6). At the top sensors, vertical maximum accelerations ranged from more than 500 m s^{-2} for short distances of 7 m or large charge sizes of 8.5 kg to 10 m s^{-2} for large distances up to 41.8 m and small charge sizes of 2.5 kg. Maximum accelerations at the deepest sensors correspondingly ranged from 50 m s^{-2} to 2 m s^{-2} with increasing distance from the first to the last pit. The uppermost accelerometer in each pit and in each experiment showed a high frequency first peak which was distorted and attenuated at the locations of the lower accelerometers (Fig. 7). During some of the experiments, before the arrival of the distinct high amplitude wave, a first low amplitude high frequency wavelet was observed (Fig. 8). This first wave was not visible at deeper sensor locations (Fig. 7). The first prominent wave was usually superimposed by waves with smaller amplitudes and often followed

Table 3
Snowpack characteristics of all tests during winter 2013–2014 including snow depth, wetness and stability class (according to Schweizer and Wiesinger (2001)).

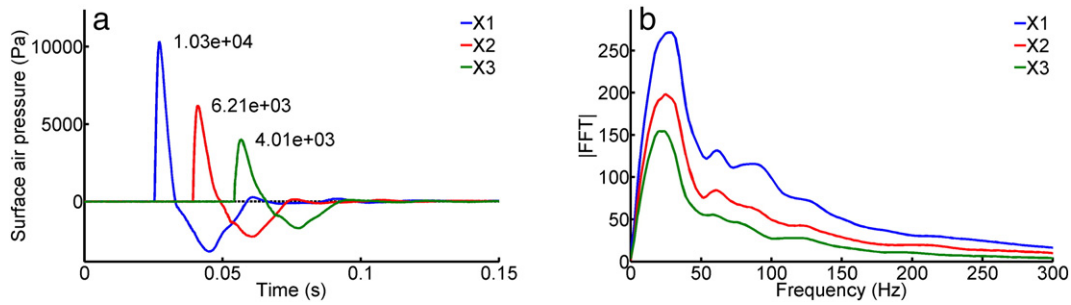| Date	Field site	Snow depth (cm)	Snowpack wetness	Stability class
12 Feb 2014	HINT	153	Dry	Good
18 Feb 2014	HINT	176	Dry	Good
25 Feb 2014	HINT	177	Dry	Good
27 Feb 2014	HINT	187	Dry	Good
25 Mar 2014	HINT	145	Wet	Good
26 Mar 2014	HINT	151	Wet	Good

Fig. 4. Typical air pressure waves (left) and their frequency content (right, Fast Fourier Transform: FFT) measured at three different distances from the blast (X1: 12.3 m, X2: 17.3 m, X3: 22.5 m). Data from 27 February 2014, test 1.

by waves with small amplitudes that arrived later at the sensor (Fig. 8). During some experiments, a second major wave reached or even exceeded the amplitude of the first wave (Fig. 9). The horizontal signals show the same features as the vertical accelerations but with smaller amplitudes (Fig. 7). As for the air pressure, the frequency content illustrates the decay in the higher frequency range with increasing depth within the snowpack (Fig. 10).

For each pit, vertical and horizontal components of the acceleration were plotted against the depth of the respective sensor and fitted to a power law (Fig. 11). As the depth of the sensors slightly varied from pit to pit, the acceleration was then calculated for a given depth for each pit of a single experiment using these power law functions. This procedure allowed the decrease of the acceleration in a given depth with distance from the point of explosion to be determined — by again fitting a power law relation. At a depth of 0.3 m kg$^{-1/3}$ below the snow surface, for which the fits were calculated, vertical minimum and maximum accelerations on average decreased proportional to $x'^{-1.3}$ and $x'^{-1.0}$, respectively, but scatter was large. Horizontal minimum and maximum accelerations decreased more strongly proportional to $x'^{-2.1}$ and $x'^{-1.9}$, respectively. Considering minimum, maximum, horizontal and vertical accelerations, the decay of accelerations between consecutive tests with equal charge mass and charge elevation above the snow surface was for most tests approximately the same considering slight variations in charge elevation, charge masses and horizontal position of the point of explosion.

Displacement velocity is the speed, with which a particle in the snowpack moves due to loading by a wave as e.g., caused by an explosion. Displacement velocity is derived by integrating the snowpack acceleration with respect to time. Velocity was calculated for all experiments. Fig. 12 shows typical velocities for a certain distance from the point of explosion. Velocities were usually largest close to the surface and in vertical direction and decayed with depth within the snowpack

with a few exceptions. As for the accelerations and the air pressures, a power law was fitted to describe the relation between displacement velocity and depth of the sensor within the snowpack. Then, these functions were again fitted with a power law using the scaled horizontal distance from the point of explosion and a certain depth within the snowpack. Vertical minimum and maximum displacement velocities decayed proportional to $x'^{-1.2}$ and $x'^{-0.8}$, respectively. The respective horizontal displacement velocities decreased proportional to $x'^{-1.8}$ and $x'^{-1.9}$, respectively.

Displacements in vertical and horizontal directions of the different sensors were calculated by integrating displacement velocity with respect to time. Because sensor noise caused increasing displacement even after the wave had passed, the signal was cut manually before and after the main contributions of the displacement velocity to displacement.

Maximum displacement reached a maximum of a few millimeters but decreased strongly with depth within the snowpack (Fig. 13). Final, remaining displacement was in the range of a few millimeters for the uppermost sensors but usually small for all other sensors. As for acceleration, displacement velocity and air pressure, a power law was used to fit the maximum and minimum displacement amplitude with increasing depth. Then, a power law was used to determine maximum displacement depending on the horizontal distance from the point of explosion.

Final vertical and horizontal displacements were in the range of 10^{-4} to 10^{-5} m, with some measurements up to a maximum of 1 cm.

Microphones were installed slightly displaced horizontally from the accelerometers by a distance of 0.35 m up to 1.35 m in order to not disturb the snowpack above the sensors. With a few exceptions, the high amplitude wave within the snowpack arrived 5 to 16 ms earlier at the accelerometers than the air pressure wave at the microphone. Often, a second major wave (Figs. 7a to c and 9) was visible in the signal. This wave decayed in amplitude with distance and depth within the snowpack. The time delay of this wave compared to the first high amplitude wave was between 0.05 and 0.09 s.

3.4. Weak layer failure

We made 106 observations of pit walls with cameras during the winter season 2013–2014. We observed 20 failures, some of them including multiple failures at different depths (Fig. 14). Most failures were observed in non-persistent weak layers since no prominent weak layers existed in the generally stable snowpack. Failures occurred immediately after arrival of the air pressure wave which could be identified by a snow spray. In most cases, failure layers were close to the snow surface but occasionally failures deep in the snowpack (up to 1 m below the snow surface) were recorded in tests with either large charge sizes or pits close to the point of explosion. Only 6 failures were observed with depths larger than 0.5 m below the snow surface.
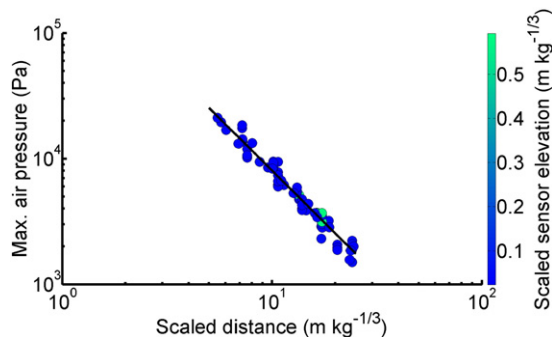

Fig. 5. Maximum air pressure of all experiments vs. scaled horizontal distance from the point of explosion. Marker fill color shows the elevation of the microphone above the surface ($N = 25$). The line indicates a power law fit according to Eq. (2) with exponent $b = -1.66$.

Table 4
Summary of all experiments indicating charge elevation, charge mass, air pressure wave propagation speed (c_{air}) between the point of explosion X0 and pit X1, pit X1 and pit X2, and pit X2 and pit X3. The distances were horizontally measured between the point of explosion and the respective pit.

Date	Test no.	Charge elevation (m)	Scaled charge elevation (m kg$^{-1/3}$)	Charge mass (kg)	Distance (m)			c_{air} (m s^{-1})		
					X1	X2	X3	Det–X1	X1–X2	X2–X3
6 Feb 2014	1	2	1.17	5	19.2	29.4	41.2	397	340	352
6 Feb 2014	2	2	1.17	5	19.2	29.4	41.2	396	338	352
6 Feb 2014	3	1	0.58	5	19.2	29.4	41.2	407	332	332
6 Feb 2014	4	0	0.00	5	19.2	29.4	41.2	386	336	349
12 Feb 2014	1	1.85	0.91	8.5	9.6	19.5	29.7		327	
12 Feb 2014	2	1.85	1.08	5	9.6	19.5	29.7		326	
12 Feb 2014	3	1.85	1.08	5	5.5	15.3	25.4			
12 Feb 2014	4	1.5	0.88	5	21.9	31.9	41.8		331	
18 Feb 2014	1	2	1.17	5	20.0	30.0	40.0	366	370	333
18 Feb 2014	2	3	1.75	5	15.0	25.0	35.0	398	379	335
18 Feb 2014	3	2	1.17	5	15.0	25.0	35.0			
18 Feb 2014	4	2	1.17	5	15.0	25.0	35.0	410	369	338
18 Feb 2014	5	1	0.58	5	15.0	25.0	35.0	415	369	334
25 Feb 2014	1	2	1.23	4.25	17.3	28.0	28.0	436	347	
25 Feb 2014	2	2	1.23	4.25	17.3	28.0	28.0	437	345	348
25 Feb 2014	3	2	1.17	5	17.3	28.0	28.0	435	351	355
25 Feb 2014	4	3	1.85	4.25	17.3	28.0	28.0	432	351	355
25 Feb 2014	5	2	1.23	4.25	12.3	23.0	23.0			
25 Feb 2014	6	2	1.17	5	12.3	23.0	23.0	494	359	363
25 Feb 2014	7	2	1.17	5	12.3	23.0	23.0	518	359	363
27 Feb 2014	1	1	0.62	4.25	12.3	17.3	22.5	490	358	343
27 Feb 2014	2	1	0.62	4.25	12.3	17.3	22.5	497	355	345
27 Feb 2014	3	1.9	1.17	4.25	12.3	17.3	22.5	496	364	347
27 Feb 2014	4	2	1.23	4.25	12.3	17.3	22.5	472	362	344
27 Feb 2014	5	2	1.17	5	12.3	17.3	22.5	505	363	347
27 Feb 2014	6	3	1.75	5	12.3	17.3	22.5	497	370	351
27 Feb 2014	7	3	1.75	5	12.3	17.3	22.5	505	366	349
27 Feb 2014	8	2	0.93	10	12.3	17.3	22.5	534	377	
25 Mar 2014	1	2	1.47	2.5	11.8	21.7	32.1	452	347	333
25 Mar 2014	2	2	1.17	5	11.8	21.7	32.1	481	349	333
25 Mar 2014	3	2	1.02	7.5	11.8	21.7	32.1	534	355	335
25 Mar 2014	4	2	0.93	10	11.8	21.7	32.1	547	358	339
26 Mar 2014	1	1	0.74	2.5	12.2	17.2	22.8	452	350	339
26 Mar 2014	2	2	1.17	5	12.2	17.2	22.8	489	352	
26 Mar 2014	3	2	1.17	5	12.2	17.2	22.8	495	352	
26 Mar 2014	4	1	0.62	4.25	12.2	17.2	22.8	521	352	
26 Mar 2014	5	1	0.62	4.25	7.0	11.9	17.6		373	
26 Mar 2014	6	0	0.00	8.5	7.0	11.9	17.6		373	

4. Discussion

4.1. Air pressure

Air pressure showed a typical decay while traveling above the snow surface. The decay is due to a combination of spherical spreading as well as a change in reflection of wave energy off the porous snow surface. The amplitude of a spherical wave decays proportional to r^{-1}, where r is the radius from the source. We observed a decay proportional to $x'^{-1.1}$ to $x'^{-2.1}$. The stronger decay than in the case of a spherical spreading is caused by charge elevation which causes a different incident angle on the snowpack and hence a different reflection and a different effect on the air pressure measured; in addition, snow surface properties contribute to the variation.

The wave velocities above the speed of sound, increasing with decreasing distance from the point of explosion indicate that we measured to some extent in the range of shock propagation, which is a non-adiabatic process and causes a stronger decay. Miller et al. (2011) numerically modeled the effect of explosions on a snowpack. Their modeled air pressure was higher than the predicted open air pressure. Our values of air pressure were in the range of an open air blast as shown in Miller et al. (2011). Low density snow at the top of the
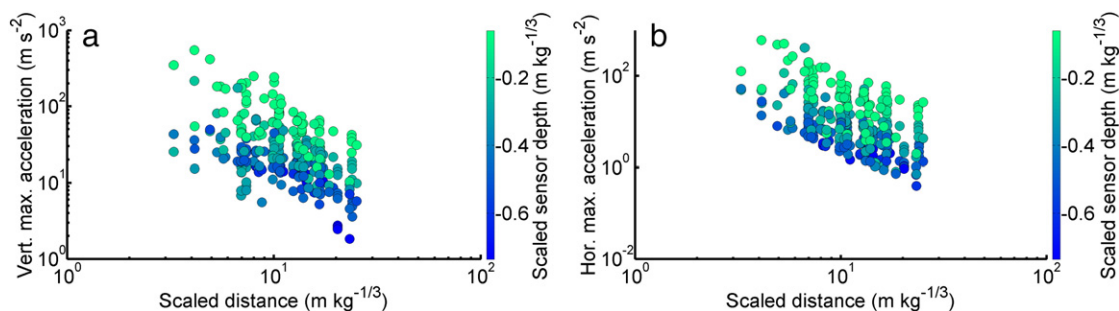

Fig. 6. (a) maximum vertical and (b) horizontal accelerations of all experiments with increasing scaled horizontal distance from the point of explosion. Marker fill color shows the scaled accelerometer depth below snow surface.
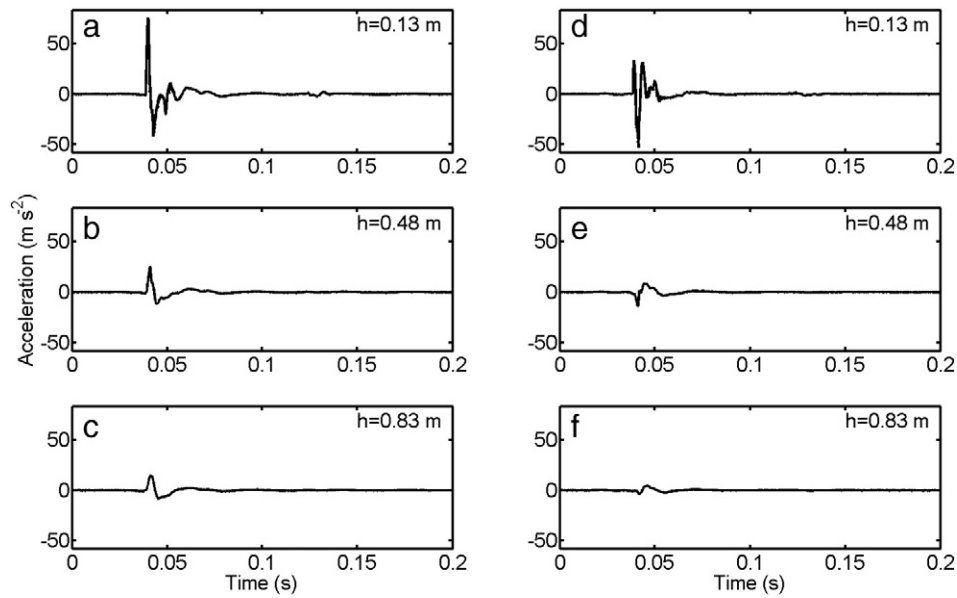
Fig. 7. Vertical (a, b, c) and horizontal (d, e, f) accelerations with increasing depth at a horizontal distance of 17.3 m from the point of explosion. Data from 27 February 2014, test 1.

snowpack and hence the porous interface has a similar impedance as air and does not reflect the incoming wave strongly which is why the expansion is more similar to an open air blast.

We measured lower air pressure values than Mellor (1965) reported, probably due to less effective explosives used in our experiments which is indicated by the very high detonation speeds he mentioned. The air pressures reported in Mellor (1973) but originally measured by Ingram (1962) were also higher than our data possibly as well due to the different type of explosive used. Ingram (1962) showed a decay of air pressure which corresponds reasonably well with our results (Table 5). We measured a stronger decay than Gubler (1976) who used a charge of 1 kg of Plastex detonated 1 m above the snow surface. Albert and Hole (2001) investigated blast noise propagation above a snowpack which is in very good agreement with our data. They suggested that rather the influence of the snowpack is relevant for the magnitude of the decay than shock effects close to the point of explosion.

Air temperatures measured during the experiments were ranging from −4 to 0 °C so that the sound speed in air is expected to range from 329 to 331 m s^{-1}. In the vicinity of the point of explosion, air pressure wave speeds were (markedly) higher than the sound speed (Table 4). Further from the point of explosion, wave speeds decreased and were in the range of the expected sound speed. Speeds peaked at 547 m s^{-1} for distances measured between the point of explosion and the closest pits (5.5 to 19.2 m) decreasing to 332 m s^{-1} between pits furthest from the point of explosion (17.6 to 41.8 m). Speeds at closer range indicate that we measure to some extent within the range of

inelastic shock expansion as shock propagation speeds are higher than the speed of sound.

4.2. Acceleration, displacement velocity and displacement

For explosions above the surface, Gubler (1976) reported ice lattice accelerations for a snowpack deeper than 1.2 m and the sensor at depths smaller or equal to half the snow depth. Our results show comparable values for the middle accelerometer in Fig. 7 considering the larger charges employed in our experiments. Maximum vertical accelerations with scaled distance from the point of explosion decayed proportional to x'^{-1} on average at 0.3 m kg$^{-1/3}$ depth within the snowpack for the experiments performed under dry snowpack conditions — but scatter was large. Maximum horizontal accelerations decreased even more rapidly with distance proportional to $x'^{-2.1}$ on average. A strong decay in amplitude of radial accelerations was also observed for close ranges from the point of explosion by Bones et al. (2012) ranging from $x'^{-1.25}$ to x'^{-3} depending on the scaled charge height. Consecutive testing with same charge sizes and charge elevations above the snowpack had neither a significant influence on maximum acceleration nor maximum air pressure. The snowpack was probably not affected sufficiently to cause any difference in the wave propagation characteristics directly above or within the snowpack. Only at short ranges settlement of the snow surface due to compaction could be observed after subsequent experiments. Actual crater formation was only observed for zero or small charge elevation above the snow surface which is in
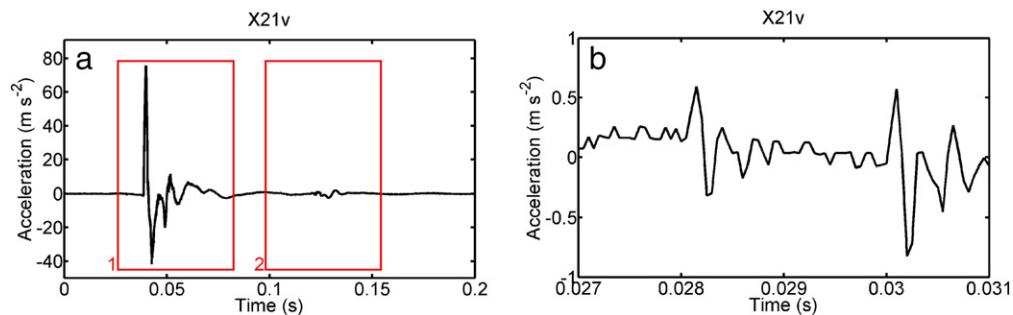

Fig. 8. (a) Example of vertical acceleration at 0.13 m below the snow surface and 17.15 m horizontal distance from the point of explosion. In panel 1 a wave arrives preceding the main, high amplitude wave. In panel 2 the arrival of a later wave propagating through the snowpack is highlighted. (b) Excerpt showing the wave preceding the main, high amplitude wave (in panel 1 of panel a). Data from 27 February 2014, test 1.
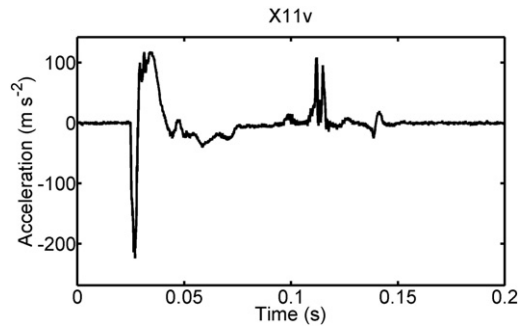
Fig. 9. Vertical acceleration at 0.13 m below the snow surface at the first snow pit with a distinct second wave with similar positive amplitude as the first wave. Data from 27 February 2014, test 4.

Fig. 11. Measured and fitted (power law) maximum vertical acceleration with scaled sensor depth within the snowpack at three different scaled horizontal distances from the point of explosion (X1: 8.2 m, X2: 14.4 m, X3: 20.3 m) on 18 February 2014, test 3.

agreement with the results of Frigo et al. (2012) and Strange et al. (1961) who show decreasing crater size with increasing charge elevation.

The complex wave propagation characteristics in snow caused by a point source explosion above the snowpack hamper the interpretation of the recorded signals from only few selected locations. In a snowpack, three different wave modes occur as described by Johnson (1982). In addition, surface waves exist caused by the shallow incident angle of the air pressure wave at the investigated distances from the point of explosion. Furthermore, these three different wave types traveling within the snowpack and the surface waves are generated by the air pressure hitting the surface at each point between the point of explosion and the measurement location — so that the recorded signal is a superposition of many different waves and wave types. It is therefore not possible to determine with certainty which of the many waves observed in the accelerometer signal corresponds to which kind of wave mode and where it originated from. With the size of the acceleration sensor, we presumably measured a combined acceleration of the ice lattice and the air wave within the pores. The contribution of these to the overall acceleration is not known. The wave which was arriving before the high amplitude wave in some experiments could not be seen in all of the experiments due to the probably very low amplitude in the range of signal noise. The early arrival time might correspond to the high velocity of the first dilatational wave through the ice skeleton; however, one would not expect such low amplitudes for this type of wave. The
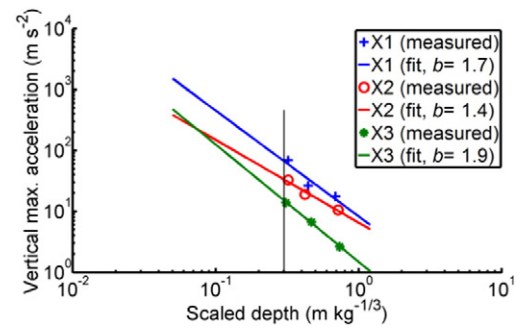
waves that arrived later at the sensor might originate from the air pressure wave hitting the snow surface at different locations and being partly transmitted into the snowpack.

Maximum and final displacements recorded at the top sensors within the snowpack were higher than those buried deeper. Horizontal final displacement was probably due to low density snow close to the snow surface that was deformed, whereas vertical final displacement was mainly due to compaction of the snowpack. As no persistent weak layers existed that could have failed and collapsed, large vertical displacements were not observed; instead we only recorded small values of vertical displacement in the range of 10^{-4} to 10^{-5} m. Due to higher densities in greater depths within the snowpack and consequently higher elastic moduli, displacements were negligible in these regions. Very high displacements, in one case we measured almost 1 cm, were probably caused by snow densification in the low density snow at the top of the snowpack or by collapse of a layer. As there were hardly any persistent weak layers present that would allow for the latter, the first reason is more likely.

Gubler (1976) calculated displacement velocities and displacement from acceleration data. His vertical displacement velocities decayed much stronger ($x'^{-1.39}$) with horizontal distance from the point of explosion than our data suggest ($x'^{-0.51}$ on average). However, the data presented by Gubler (1976) resulted from measurements at a depth of half or smaller than half the snow depth from the surface. The strong decay with depth within the snowpack might influence the spreading
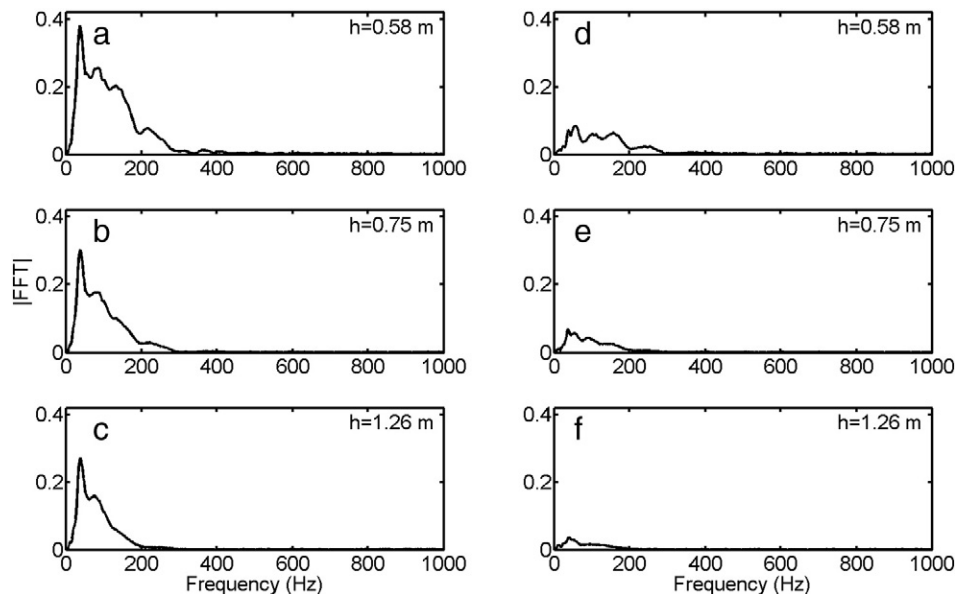

Fig. 10. Frequency content of the vertical (a, b, c) and horizontal (d, e, f) accelerations with increasing depth from top to bottom, at a horizontal distance of 20.0 m from the point of explosion. Data from 18 February 2014, test 1.
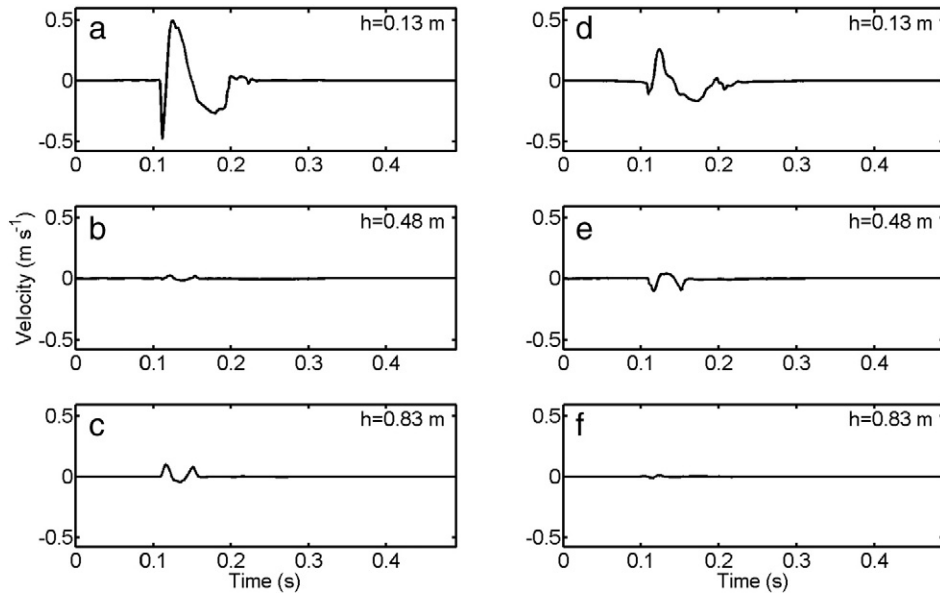
Fig. 12. Example of vertical (a, b, c) and horizontal (d, e, f) displacement velocity with increasing depth (top to bottom) at a horizontal distance of 12.3 m from the point of explosion. Data from 27 February 2014, test 4.

at a certain depth with horizontal distance from the point of explosion. The decay of the horizontal displacement velocity presented by Gubler (1976) is in good agreement with our findings ($x'^{-1.8}$ and $x'^{-1.9}$ on average, respectively).

Vertical displacements measured by Gubler (1976) for a sensor 'at half or less than half the depth' of the snowpack from the surface was ranging from 4×10^{-4} to 4×10^{-5} m. This is in good agreement with what we measured except for the top sensors if close to the point of explosion.

4.3. Acceleration–air pressure relation

In the vast majority (21) of the 25 experiments with pressure and acceleration measurements, the exponent of the fitted power law was smaller for the maximum vertical acceleration at 0.3 m scaled depth

($x'^{-1.0}$) compared to the air pressure ($x'^{-1.6}$), the difference being 0.71 on average (Fig. 15). We believe that this is due to surface waves that expand cylindrically within the snowpack. The amplitude of a cylindrical wave should decay with $x^{-0.5}$. Higher decay rates are presumably due to a mixed spherical–cylindrical expansion and due to attenuation of the wave within the snowpack.

4.4. Wave arrival time

The minimum time an air pressure wave needs to cover the horizontal distance between a point on the snow surface directly above the accelerometer and the microphone is the ratio of the maximum microphone offset divided by the slowest air pressure speed measured (350 m s^{-1}). This yields a time delay of 3×10^{-3} s which is shorter than the arrival time delay of the wave at the microphone compared
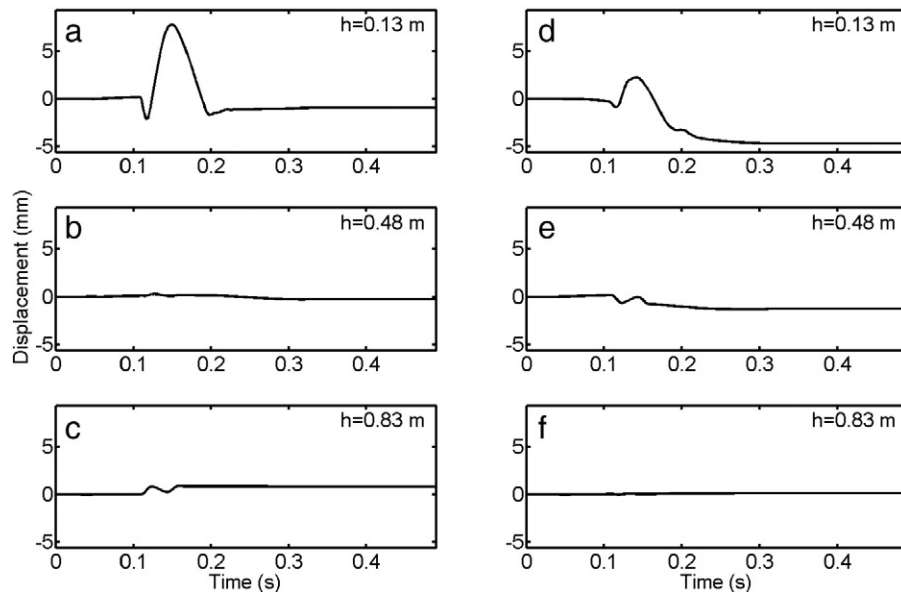

Fig. 13. Example of vertical (a, b, c) and horizontal (d, e, f) displacement with increasing depth (top to bottom) at a horizontal distance of 12.3 m from the point of explosion. Data from 27 February 2014, test 4.
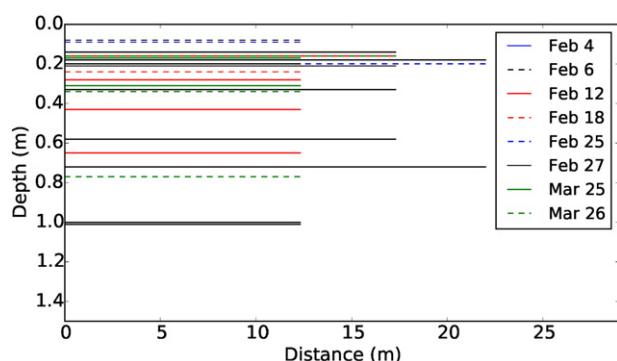
Fig. 14. Lines indicating the maximum horizontal distance from the point of explosion and depth below snow surface where failure was still observed.

to the accelerometer. Arrival of the first high amplitude wave was expected to be before the air pressure wave for the top sensors because the wave arriving at the sensor was resulting from the air pressure waves hitting the snow surface at a shallow angle of incidence closer to the point of explosion. Due to the higher density of the snow compared to air, the wave traveled faster within the snowpack. Lower sensors showed the same arrival time differences. This was probably due to the increasing density and hence velocity with depth within the snowpack which compensated for the longer distances the wave traveled. During some experiments there were waves before the major wave with very weak amplitude compared to the main wave (Fig. 8). These waves may be explained either by the fast dilatational wave traveling through the ice skeleton (Johnson, 1982) or a surface wave that propagates as a cylindrical wave at higher velocity than the air pressure wave but is attenuated strongly with depth within the snowpack.

The second high amplitude wave (Fig. 9) is not believed to be the result of a reflection at the snow–soil interface, where a large impedance mismatch is expected, as the amplitudes of the waves decay strongly with depth within the snowpack. We believe that these waves were slow waves (Johnson, 1982) traveling through the pore space of the snowpack.

Ground motion did not seem to have had an influence on the snowpack as accelerations and derived parameters strongly decayed with depth and no waves with decreasing amplitude from bottom to top were recorded that exceeded the waves caused by the air blast transferred to the snowpack.

4.5. Weak layer failure

Very close to the point of explosion, the shock caused by a standard charge (e.g., a few kilograms TNT equivalent) will be sufficiently strong to fail almost any given weak layer down to the relevant depth for avalanche release. However, a weak layer may not exist or the slab–weak layer combination may not be prone to crack propagation at a close distance. Hence it is important whether a given explosion is strong enough to cause a weak layer to fail further away from the point of explosion, i.e., rather in the range of elastic wave propagation.

During the experiments in winter 2013–2014 we observed that weak layer failure was always immediate after the air pressure wave

Table 5
Power law exponent b for the air pressure decay reported in different studies.

	Exponent b
Ingram (1962), Mellor (1973)	1.43
Gubler (1976)	1.125
Albert and Hole (2001)	1.5 to 1.9
Present study	1.1 to 2.1

had passed the point of observation. With increasing distance from the point of explosion, failure became less frequent.

In the single experiment described by Simioni and Schweizer (2013), even at 25 m from the point of explosion, the observed weak layer failure occurred 0.4 s after the arrival of the air pressure wave at the point of observation (pit). We suppose that the failure in this single experiment from the season 2012–2013 was not caused by the incident air pressure wave impacting on the snow surface close to the pit. The short distance and the high wave velocities in snow would not account for the time delay between the snow spray caused by the passing air pressure wave and the observed failure at the weak layer. Failure was rather caused by the air pressure wave impinging on the snow surface closer to the point of explosion and being partly transferred to the snowpack. One of the excited wave modes (dilatational or shear) then locally failed the weak layer and crack propagation started. The low velocity of crack propagation, previously reported values were in the range of 8 to 42 m s^{-1} (van Herwijnen and Birkeland, 2014; van Herwijnen and Schweizer, 2011), was then responsible for the time delay.

Hence, there seem to be two distinctly different types of mechanisms causing weak layer failure at distances of several tens of meters from the point of explosion. The relatively poor snowpack stability during winter 2012–2013 compared to the winter 2013–2014 supports this finding. During winter 2013–2014 no crack propagation occurred, but failure was caused directly at the observed distance. The good snowpack stability conditions did not favor crack propagation.

Weak layer failure was not detected above 14 m kg$^{-1/3}$ scaled horizontal distance from the point of explosion. During some experiments, no failure was observed close to the point of explosion even if failure was detected further from the point of explosion. Either, a suitable weak layer was not present closer to the point of explosion, or, more likely, failure could not be detected by visual inspection. Failure close to the snow surface was detectable because the slab was slightly lifted by the negative pressure impulse. Deeper in the snowpack failure was usually only visible with major vertical displacement (collapse). When failure only occurred at the farer pit locations, we assumed that the same layer was failing at closer pit locations because of the spatially uniform snowpack though it could not be observed.

The observed rare occurrence of failures deeper in the snowpack – six out of 20 – and further from the point of explosion corresponded well with the low accelerations, displacement velocities and displacements measured at these locations.

5. Conclusions

We performed field experiments using avalanche control explosives on a flat, snow-covered study site. We measured near-surface air pressure at different distances from the explosion using three locations on each test ranging from 7 m to 43 m horizontal distance. Within the snowpack, we recorded snowpack accelerations at these distances and at different depths within the snowpack ranging from 0.1 m to 1.3 m below the snow surface. We monitored pit walls at these locations with high speed cameras to visually identify weak layer failure. Due to the generally good stability of the snowpack, only few failures were observed, mainly at closer range from the point of explosion.

Air pressure decreased rapidly with scaled distance from the point of explosion proportional to $x'^{-1.66}$, indicating the influence of the snowpack on the decay of the amplitude. Air pressure wave propagation speeds were well above sound speed for short distances from the point of explosion due to non-linear effects in shock wave propagation (up to 547 m s^{-1}). Wave propagation speeds decreased with distance to sonic level. Accelerations decreased rapidly with depth within the snowpack and, for a given depth, with distance from the point of explosion (on average proportional to x'^{-1} at 0.3 m scaled depth for vertical maximum accelerations) due to geometrical spreading and attenuation due to the poro-elastic character of snow. Air pressure usually decayed
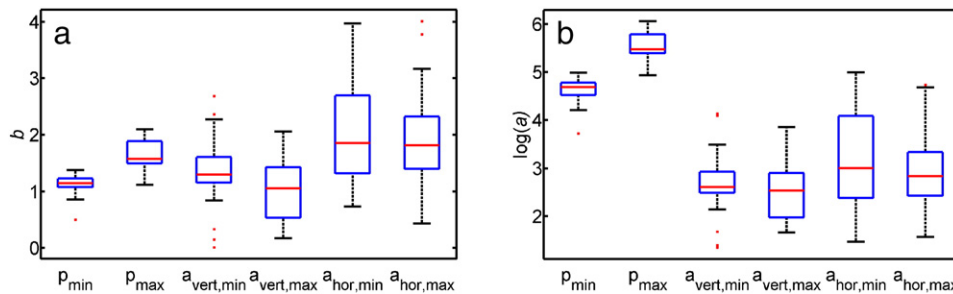
Fig. 15. Parameters of power law fits: (a) coefficients b and (b) $\log(a)$ for air pressure and acceleration with scaled horizontal distance from the point of explosion. Boxes span the interquartile range from 1st to 3rd quartiles with a horizontal line showing the median. Whiskers extend to the most extreme data points not considered outliers (red dots) within 1.5 times the interquartile range above the 3rd and below the 1st quartile. Number of cases varies between 25 and 29.

stronger than maximum vertical acceleration. This finding indicates that some wave modes within the snowpack propagate as surface waves and expand cylindrically. Vertical accelerations were usually stronger in amplitude than horizontal ones.

The air pressure waves arrived at the microphones with a time delay compared to the arrival time of the waves within the snowpack at the top accelerometers, taking into account the horizontal offset of the microphone. This delay was expected due to higher wave velocities within the snowpack. However, waves at lower sensors did not arrive significantly later than at the top sensor. This, together with the strong decay within the snowpack, probably indicates a surface wave propagating through the snowpack. Early low amplitude waves observed might be due to the fast wave mode propagating through the ice lattice. Later waves, as often observed, might be due to a slow wave, probably traveling through the air pores, rather than due to reflections lower in the snowpack as their amplitude decreased strongly with depth and time delays were large. Consecutive testing with equal charge sizes and charge elevations did not result in different air pressure or acceleration response.

Displacement speeds were usually less than 1 m s^{-1} for the top sensor and decayed strongly with depth within the snowpack and distance from the point of explosion. Compared to the top sensor, the middle and bottom sensors showed negligible displacement speeds.

Maximum displacements reached 1 cm for the top sensors during some experiments but were usually smaller (10^{-4} to 10^{-5} m). Displacements were negligible deeper in the snowpack. Final displacements were in the same range as the maximum displacements. The resulting small displacements were due to the absence of persistent weak layers with notable collapse heights.

Whereas our setup and instrumentation allows recording the response of the snowpack to explosive loading with good accuracy and high temporal resolution and hence provides insight into the complex wave propagation behavior in and above a snowpack, detailed propagation patterns cannot be observed with a few measuring locations only.

Failure evaluation using high speed cameras has to our knowledge not been used in avalanche control experiments using explosives and seems to be a method with relevant informative content. Even under conditions with no persistent weak layer but mainly failures at layer interfaces with hardly any collapse height, the method allowed to determine weak layer failure by visually inspecting the single video stills individually. The method allowed distinguishing between two types of weak layer failure: (1) failure caused by the direct impact of the air pressure wave above the point of observation, and (2) failure caused by crack propagation initiated at a distance closer to the point of explosion than the point of observation as manifested by an arrival time delay.

Though the markers inserted into the pit wall would allow for particle tracking, the snow spray caused by the air pressure wave and single markers moving relative to the pit wall did not allow the pit wall displacements to be evaluated quantitatively. Furthermore, in order to use the recordings for particle tracking, the frame rate of our cameras

was too low compared to the propagation speed of dilatational and shear waves in a snowpack and the snow spray inhibited real time tracking. However, particle tracking may still be useful for determining the total displacements.

We will continue performing field experiments on avalanche control to cover different snowpack conditions, new types of explosives and different control techniques including gas exploders. In addition, we will use our data to model wave propagation caused by explosions and deflagrations employing different modeling techniques (e.g., Miller et al., 2011; Sidler et al., 2010). Small scale experiments are planned to gain a better understanding of wave propagation principles in a snowpack.

Acknowledgments

References

Albert, D.G., Hole, L.R., 2001. Blast noise propagation above a snow cover. J. Acoust. Soc. Am. 109 (6), 2675–2681.

Albert, D.G., Decato, S.N., Carbee, D.L., 2008. Snow cover effects on acoustic sensors. Cold Reg. Sci. Technol. 52 (2), 132–145.

Albert, D.G., Taherzadeh, S., Attenborough, K., Boulanger, P., Decato, S.N., 2013. Ground vibrations produced by surface and near-surface explosions. Appl. Acoust. 74 (11), 1279–1296.

Binger, C., Nelsen, J., Olson, K.A., 2006. Explosive shock wave compression in snow: effects of explosive orientation and snowpack compression. In: Gleason, J.A. (Ed.), Proceedings ISSW 2006. International Snow Science Workshop, Telluride CO, U.S.A., 1–6 October 2006, pp. 592–597.

Bones, J., Miller, D., Savage, S., 2012. An experimental dynamic response study of hard slab seasonal snow to explosive control. International Snow Science Workshop ISSW 2012, Anchorage AK, U.S.A., 16–21 September 2012, pp. 142–148.

Cardu, M., Chiaravalloti, L., Chiaia, B., Cornetti, P., Frigo, B., 2008. A coupled stress and energy criterion for natural and artificial triggering of dry snow slab avalanches. 42nd US Rock Mechanics Symposium and 2nd U.S.–Canada Rock Mechanics Symposium, San Francisco, U.S.A., 29 June–2 July 2008.

Chernouss, P., Fedorenko, Y., Barashev, N., Mokrov, E., 2006. A study of blasting-induced snow instabilities and avalanche releases. In: Gleason, J.A. (Ed.), Proceedings ISSW 2006. International Snow Science Workshop, Telluride CO, U.S.A., 1–6 October 2006, pp. 598–606.

Cooper, P.W., 1996. Explosives Engineering. Wiley-VCH, New York (480 pp.).

Denoth, A., 1994. An electronic device for long-term snow wetness recording. Ann. Glaciol. 19, 104–106.

Fierz, C., Armstrong, R.L., Fierz, C., Armstrong, R.L., Durand, Y., Etchevers, P., Greene, E., McClung, D.M., Nishimura, K., Satyawali, P.K., Sokratov, S.A., 2009. The international classification for seasonal snow on the ground. HP-VII Technical Documents in Hydrology 83. UNESCO-IHP, Paris, France (90 pp.).

Frigo, B., Chiaia, B., Cardu, M., Giraudi, A., Godio, A., Rege, R., 2010. Experimental analysis of snowpack effects induced by blasts. International Snow Science Workshop ISSW, Lake Tahoe, CA, U.S.A., 17–22 October 2010, pp. 66–71.

Frigo, B., Chiaia, B., Cardu, M., 2012. Snowpack effects induced by blasts: experimental measurements vs theoretical formulas. International Snow Science Workshop ISSW 2012, Anchorage AK, U.S.A., 16–21 September 2012, pp. 943–947.

Gubler, H., 1976. Künstliche Auslösung von Lawinen durch Sprengungen 32. Swiss Federal Institute for Snow and Avalanche Research, Davos, Switzerland.

Gubler, H., 1977. Artificial release of avalanches by explosives. J. Glaciol. 19 (81), 419–429.

Gubler, H., 1993. Artificial release of avalanches. Proc. Int. Symp. on Avalanche Control, Nagaoka, Japan, 11–12 September 1992. Japanese Society of Snow and Ice, Nagaoka, Japan, pp. 102–130.

Ingram, L.F., 1962. Air blast in an arctic environment. Technical Report no. 2-597. US Army Waterways Experiment Station, Vicksburg, MS, U.S.A.

Johnson, J.B., 1982. On the application of Biot's theory to acoustic wave propagation. Cold Reg. Sci. Technol. 6 (1), 49–60.

Johnson, J.B., 1990. Estimates of shock wave attenuation in snow. Report 90-8. US Army CRREL, Hanover, NH, U.S.A.

Johnson, J.B., Solie, D.J., Brown, J.A., Gaffney, E.S., 1993. Shock response of snow. J. Appl. Phys. 73 (10), 4852–4861.

Johnson, J.B., Solie, D.J., Barrett, S.A., 1994. Response of seasonal snow to explosive loading. Ann. Glaciol. 19, 49–54.

McClung, D.M., Schaerer, P., 2006. The Avalanche Handbook. The Mountaineers Books, Seattle, WA, U.S.A. (342 pp.).

Mellor, M., 1965. Explosions and snow. Cold Regions Science and Engineering, Part III, Section A3a. CRREL, Hanover, NH, U.S.A. (34 pp.).

Mellor, M., 1973. Controlled release of avalanches by explosives. In: Perla, R. (Ed.), Advances in North American Avalanche Technology: 1972 Symposium. USDA Forest Service, General Technical Report RM-3, pp. 37–49.

Miller, D.A., Tichota, R.G., Adams, E.E., 2011. An explicit numerical model for the study of snow's response to explosive air blast. Cold Reg. Sci. Technol. 69 (2–3), 156–164.

Schweizer, J., Jamieson, J.B., 2010. Snowpack tests for assessing snow-slope instability. Ann. Glaciol. 51 (54), 187–194.

Schweizer, J., Wiesinger, T., 2001. Snow profile interpretation for stability evaluation. Cold Reg. Sci. Technol. 33 (2–3), 179–188.

Sidler, R., Carcione, J.M., Holliger, K., 2010. Simulation of surface waves in porous media. Geophys. J. Int. 183 (2), 820–832.

Simioni, S., Schweizer, J., 2013. Assessing weak layer failure and changes in snowpack properties due to avalanche control by explosives. In: Naaim-Bouvet, F., Durand, Y., Lambert, R. (Eds.), Proceedings ISSW 2013. International Snow Science Workshop, Grenoble, France, 7–11 October 2013. ANENA, IRSTEA, Météo-France, Grenoble, France, pp. 775–778.

Sommerfeld, R.A., 1982. A review of snow acoustics. Rev. Geophys. Space Phys. 20 (1), 62–66.

Strange, J.N., Denzel, C.W., McLane, T.I., 1961. Cratering from High Explosive Charges: Analysis of Crater Data. Corps of Engineers — U.S. Army Engineer Waterways Experiment Station.

Surinach, E., Vilajosana, I., Kleemayer, K., Rammer, L., 2011. Study of the wave field generated by a gas exploder used for artificial avalanche release. Cold Reg. Sci. Technol. 66 (1), 17–29.

Tichota, R.G., Miller, D.A., Larson, R., Richmond, D., 2010. An experimental investigation of explosives and snowpack dynamic response. International Snow Science Workshop ISSW, Lake Tahoe, CA, U.S.A., 17–22 October 2010, p. 418.

Ueland, J., 1993. Effects of explosives on the mountain snowpack. Proceedings International Snow Science Workshop, Breckenridge, Colorado, U.S.A., 4–8 October 1992. Colorado Avalanche Information Center, Denver, CO, USA, pp. 205–213.

van Herwijnen, A., Birkeland, K.W., 2014. Measurements of snow slab displacement in Extended Column Tests and comparison with Propagation Saw Tests. Cold Reg. Sci. Technol. 97, 97–103.

van Herwijnen, A., Jamieson, J.B., 2007. Snowpack properties associated with fracture initiation and propagation resulting in skier-triggered dry snow slab avalanches. Cold Reg. Sci. Technol. 50 (1–3), 13–22.

van Herwijnen, A., Schweizer, J., 2011. Seismic sensor array for monitoring an avalanche start zone: design, deployment and preliminary results. J. Glaciol. 57 (202), 267–276.

van Herwijnen, A., Schweizer, J., Heierli, J., 2010. Measurement of the deformation field associated with fracture propagation in weak snowpack layers. J. Geophys. Res. 115, F03042. http://dx.doi.org/10.1029/2009JF001515.

Withers, M., Aster, R., Young, C., Beiriger, J., Harris, M., Moore, S., Trujillo, J., 1998. A comparison of select trigger algorithms for automated global seismic phase and event detection. Bull. Seismol. Soc. Am. 88 (1), 95–106.

Wooldridge, R.E., Hendrikx, J., Miller, D.A., Birkeland, K., 2012. The effect of explosives on the physical properties of snow. International Snow Science Workshop ISSW 2012, Anchorage AK, U.S.A., 16–21 September 2012, pp. 1033–1039.